Desalination and Water Treatment
www.deswater.com

doi: 10.5004/dwt.2020.24658

173 (2020) 409–419
January

Highly efficient removal of methyl blue from aqueous solution using a novel nitrogen-doped porous magnetic carbon

Yan He[a,b,*], Xinmiao Fu[a], Han Wu[b], Tianxiao Zhu[a], Shenghui Li[a], Bing Na[a], Changjun Peng[b,*]

[a]*Jiangxi Province Key Laboratory of Polymer Micro/Nano Manufacturing and Devices, School of Chemistry, Biology and Materials Science, East China University of Technology, Nanchang, 330013, China, emails: yanhe@ecit.edu.cn (Y. He), 1028915655@qq.com (X. Fu), 1358512168@qq.com (T. Zhu), 1685187637@qq.com (S. Li), bna@ecit.cn (B. Na)*

[b]*Key Laboratory for Advanced Materials and Department of Chemistry, East China University of Science and Technology, Shanghai, 200237, China, Tel./Fax: +86-21-64252630; emails: 2824853689@qq.com (H. Wu), cjpeng@ecust.edu.cn (C. Peng)*

Received 20 January 2019; Accepted 3 July 2019

ABSTRACT

Developing magnetic adsorbents with high adsorption capacity and rapid adsorption rate is one of the greatest challenges for the removal of methyl blue (MB) from aqueous media. In this work, a novel nitrogen-doped porous magnetic carbon (denoted as N-PMC) was designed and synthesized by one-step pyrolysis method. The obtained novel porous carbon N-PMC was found highly effective in removing MB from aqueous solution. The MB adsorption rate (k_2 = 1.34 mg g^{-1} min^{-1}) of N-PMC is rapid, which is 15–20 times greater than those of activated carbon. The maximum adsorption capacity of N-PMC at room temperature calculated from the Langmuir model was 1,053.5 mg g^{-1}, one of the highest values among the currently reported magenetic adsorbents. Both experimental results and the DFT calculations illustrated that the electrostatic interaction between the N heteroatoms of the N-PMC and MB, which was responsible for efficient adsorption. Furthermore, the N-PMC could be easily isolated by magnetic force and recycled at least five times without significant loss in adsorption capacity. Therefore, the convenient synthetic route, the high adsorption capacity, the rapid adsorption rate and fast separation process make the porous carbon an attractive adsorbent for removing organic dyes from aqueous solution.

Keywords: Porous magnetic carbon; Methyl blue; High adsorption; Fast; Reused

1. Introduction

Organic dyes, especially methyl blue (MB), are important chemicals widely used in rubbers, pharmaceuticals, leather, papers, varnishes and dyestuffs, and so on [1,2]. However, these chemicals are toxic even at low concentrations and raise concerns about potential negative effects on human health [3]. Therefore, appropriate methods need to be adopted to treat wastewater. Up to now, various methods are undertaken including physical, chemical, biological and adsorption treatments [4–8]. Among them, adsorption is particularly considered as an easy-operation, low cost, recyclable and high-efficiency technology to separate pollutants from water [9]. The key to adsorption technology is to choose efficient adsorbents. In the adsorbent materials, many porous materials have been extensively studied. For example, Deng et al. [10] prepared perfluorous conjugated microporous polymers with extraordinary capability for water treatment. Zhao et al. [11] synthesized silica nano-sheets obtained from vermiculite, which exhibited the adsorption potential towards methylene blue and outstanding recyclability through ethanol treatment. However, all of

* Corresponding authors.

them require long time and complicated separation process after saturated adsorption. Hence, it is very important to develop new technologies for efficient removal of MB from aqueous media.

To solve the above problem, magnetic solid-phase extraction (MSPE) based on magnetic adsorbents has been developed as a promising technique in separation [12]. With respect to the MSPE procedure, the pollutant can be adsorbed rapidly onto the magnetic adsorbent and then be easily separated by an external magnet, which greatly simplifies the treatment procedure and enhances removal efficiency. So far, many functionalized porous materials with distinct magnetic property have been applied in removal of dyes, such as activated carbon [13], zeolitic imidazole frameworks [14], conjugated microporous polymers [10], and metal-organic frameworks [15]. However, these magnetic porous adsorbents often suffer from many drawbacks such as complicated synthesis process, slow adsorption rate (of the order of hours) and low adsorption capacity.

Generally, the removal efficiency for dyes would mainly depend on the functional groups on the surface of the adsorbents. The doping of a heteroatom into the carbon skeleton has attracted extensive attention because the process can tailor the surface properties of porous carbon [16]. In the past, different kinds of heteroatoms (e.g., phosphorus, boron, silicon, nitrogen, etc.)-doped carbons have been prepared and applied in various fields [17–20]. Among them, because of the unique basic sites, the nitrogen-doped carbon has attracted much attention, which can have much adsorption capacity for acidic molecules [21,22]. MB is an acidic dye. In principle, the nitrogen-doped carbon would exhibit good adsorption in MB. However, to the best of our knowledge, the application of nitrogen-doped porous magnetic carbon for MB has rarely been reported.

In this work, we designed and synthesized a novel nitrogen-doped porous magnetic carbon (N-PMC) with microspheres configuration by a simple pyrolysis method. The obtained magnetic adsorbent has an unexpectedly high adsorption capacity and fast adsorption rate for MB. Under the optimized condition, the N-PMC showed a relatively high MB adsorption capacity with 1,053.5 mg g^{-1}. The MB adsorption rate exhibited by N-PMC is 15–20 times greater than that of activated carbon. More significantly, the N-PMC could be easily isolated by magnetic force after saturated adsorption. Additionally, insights of the nature of interaction between MB with the magnetic adsorbent were also revealed by the experimental results and the DFT calculations.

2. Experimental

2.1. Reagents and materials

All purchased chemicals were of reagent grade and used without further purification. Melamine (M, 99%), resorcinol (R, 99%), formaldehyde (F, 37 wt% H_2O) and $Fe(NO_3)_3{\cdot}9H_2O$ were purchased from Aladdin Chemistry Co. Ltd. (Shanghai, China). All other solvents and methyl blue (MB, 98%) were purchased from TCI America (Boston, United States).

2.2. Preparation of nitrogen-doped magnetic carbon (N-PMC)

As shown in Fig. 1, 1.01 g melamine (M, 8 mmol) and 1.94 g formaldehyde (F, 37 wt%, 24 mmol) were slowly added in 30 mL distilled water. Then the MF mixtures were not stopped stirring at 80°C until the solution became clear. Next, 0.88 g resorcinol (R, 8 mmol) and 1.29 g formaldehyde (F, 37 wt%, 16 mmol) were also slowly added in 30 mL distilled water and then RF mixtures were heated at 40°C for 1 h. After the MF solution became clear and the temperature dropped to 40°C, the RF solution was mixed with it under continuous stirring for 30 min. 4.80 g $Fe(NO_3)_3{\cdot}9H_2O$ was dissolved in the above solution. Then the solution was transferred to Teflon-lined autoclave and under static conditions heated at

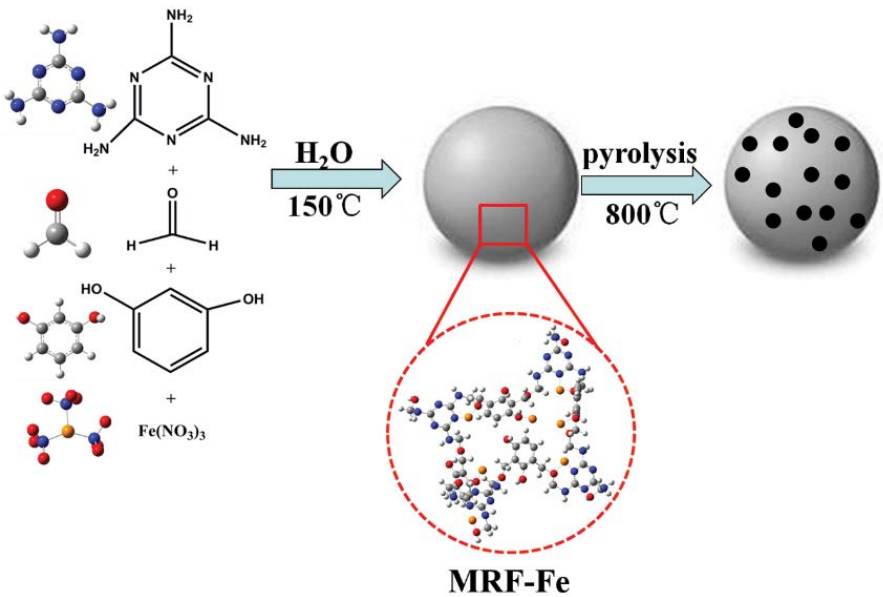

Fig. 1. Schematic representation of synthesis of nitrogen-doped porous carbon N-PMC.

180°C for 24 h. The precipitates MRF-Fe were collected by filtration and washed with distilled water, dried at 60°C under vacuum. Finally, the resultant carbon N-PMC was obtained by carbonizing the precipitates MRF-Fe at 800°C for 3 h in nitrogen flow with a heating rate of 5°C min^{-1}.

2.3. Characterization

The powder X-ray diffraction (XRD) pattern was recorded on a D/Max2550 VB/PC diffractometer (40 kV, 200 mA) using Cu Kα as the radiation. The morphology of samples was characterized by a Nova NanoSEM 450 field emission scanning electron microscope. Transmission electron microscope (TEM) images were recorded on JEM-2100. N_2 isotherms at 77 K were measured by Micromeritics ASAP 2020 (Beijing, P.R. China). Before adsorption measurements, the samples were degassed at 120°C for 24 h. The specific surface area was calculated by the Brunauer–Emmett–Teller (BET) method. The thermal stability was determined using a TGA unit (NETZSCH STA 499 F3) in N_2 atmosphere at a heating rate of 10°C min^{-1}. The Fourier transform infrared (FTIR) spectra were performed on a Nicolet iS10 FTIR spectrometer by the KBr pellet technique.

2.4. Adsorption test

2.4.1. Organic dyes adsorption

In typical adsorption experiment, 2.5 mg adsorbent was added into 5 mL of MB solution with different concentration (10–1,000 ppm) at room temperature under mechanical shaker conditions. The residual MB solution was detected using a UV–Vis spectrum at the wavelength of 600 nm [23].

2.4.2. MB adsorption kinetics

2.5 mg adsorbent was added into 5 mL MB solution with initial concentration of 10 ppm at room temperature under mechanical shaker condition. After adsorption at various time (10 s, 30 s, 1 min, 3 min, 5 min, 10 min, 20 min, 30 min), the solid was magnetically separated from the solution by an external magnet, and the filtrate was measured by UV–Vis spectrum.

2.4.3. Reusability of N-PMC

The adsorption/desorption cycles were conducted as follows: each adsorption experiment consisted of 25 mg of N-PMC with 50 mL of 10 ppm MB solution for 12 h. After the adsorption experiments, dyes-loaded powder in the flask was collected by an external magnet, and then heated in an air atmosphere at 400°C for 3 h. The above cycle was repeated five times.

2.5. DFT calculations

The DFT calculations were carried out by the Gaussian 09 software [24] with the Multiwfn program of version 3.4.1 [25]. All the molecules were fully optimized by the B3LYP method. All the atoms were employed with the 6-311G(d,p) basis set. During the calculations, no symmetry constraint was performed. In addition, frequency analysis was calculated at the same theoretical method with the same basis set. Thus, it can ensure that the configurations found are all real minima on the potential energy surface.

3. Results and discussion

3.1. Characterization of N-PMC

Fig. 2a shows the XRD pattern of N-PMC. The peak at ~26° is a characteristic diffraction peak of graphite [26], giving the formation of carbon skeleton during calcination process of the MRF-Fe. Besides, all the other peaks can be readily indexed to the phases of γ-Fe_2O_3 (JCPDS No. 39-1346) [27], α-Fe (JCPDS No. 06-0696) [28] and Fe_3C (JCPDS No. 35-0772) [28]. The formation of the magnetic particles might be interpreted by the "decomposition-reduction" processes in the pyrolysis process. Specially, in the first stage, under N_2 atmosphere, the metal precursor $Fe(NO_3)_3.9H_2O$ would be decomposed to γ-Fe_2O_3. With the carbonization temperature increased, the part of γ-Fe_2O_3 would be reduction to the Fe and Fe_3C.

In order to verify the formation of γ-Fe_2O_3 rather than Fe_3O_4, XPS was performed. As shown in Fig. 2b, two broad peaks at 725.1 and 711.0 eV are assigned to Fe2p1/2 and Fe2p3/2, respectively; additionally, the characteristic satellite peak [29] at 720.5 eV for γ-Fe_2O_3 was also observed. Thus, the formation of γ-Fe_2O_3 was rather than Fe_3O_4 during the decomposition. Moreover, the characteristic peaks [30] at 720.3 and 707.3 eV for α-Fe were observed in the XPS spectrum of N-PMC. Consequently, the γ-Fe_2O_3, α-Fe and Fe_3C are found to exist together in N-PMC. From the Raman spectra (Fig. S1), two broad peaks around 1,350 and 1,585 cm^{-1} can be observed. The peak around 1,350 cm^{-1} is usually associated with the vibrations of dangling carbon bonds at the edges of graphite defects and labelled as the D-band. The peak around 1,585 cm cm^{-1} is assigned to G-band which might be caused by the E2g mode of graphite carbon coming from the vibration of sp^2 bonded carbon atoms in a two-dimensional graphite plane [31]. I_D/I_G ratio has been used to correlate the structure of graphitic and the amorphous component of carbon materials. The I_D/I_G value is 1.04 which indicates that the as-synthesized N-PMC has crystalline graphitic carbon.

The FTIR spectrum of magnetic carbon N-PMC is shown in Fig. S2. The characteristic peaks of N-PMC appear at 1,560, 1,490 and 568 cm^{-1}. Among them, the characteristic bands at 1,560 cm^{-1} are assigned to the stretching vibration of C-N. The peak at 1,490 cm^{-1} is related to the stretching vibration of C=C. The peak at 568 cm^{-1} is related to the stretching vibration of Fe–O bonds in the crystal lattice of iron oxide. From the above data, the nitrogen atom has been doped into the N-PMC skeleton.

The morphology of N-PMC was characterized by the SEM and TEM. As shown in Fig. 3a, the polymer is composed of aggregated microspheres. Furthermore, the transmission electron microscopy (Fig. 3b) was carried out to study the morphology in detail. Obviously, the obtained N-PMC carbon has spherical structure. In addition, there are a lot of magnetic particles with ~20 to 30 nm embedded in the carbon skeleton (Fig. S3). Compared with the other porous

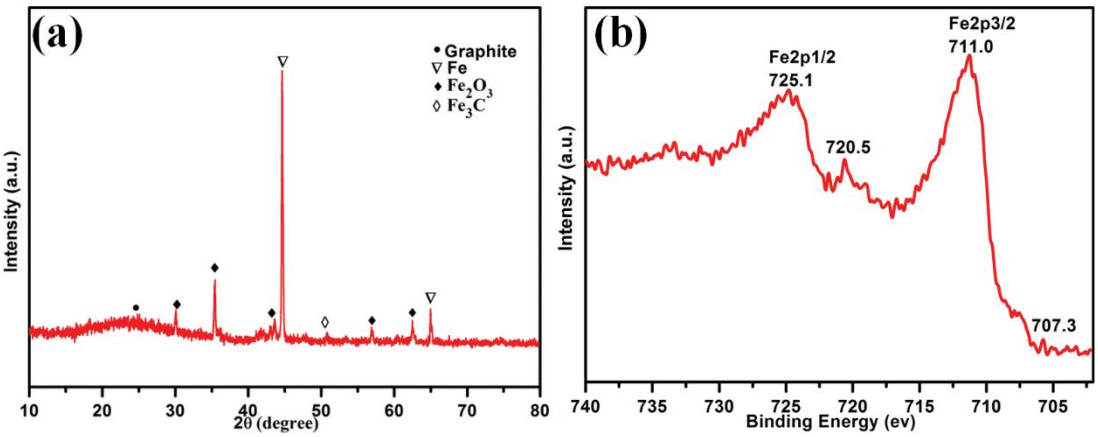

Fig. 2. (a) XRD pattern and (b) XPS spectra of magnetic polymer N-PMC.

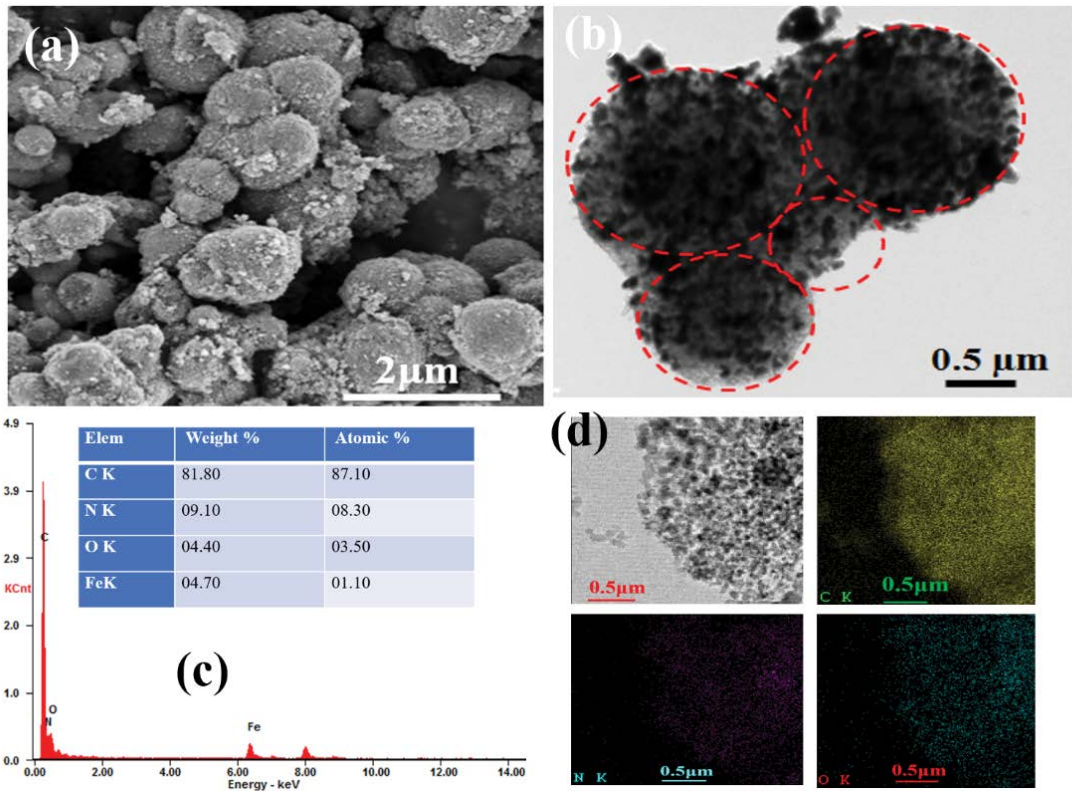

Elem	Weight %	Atomic %
C K	81.80	87.10
N K	09.10	08.30
O K	04.40	03.50
FeK	04.70	01.10

Fig. 3. SEM (a), TEM (b), EDS and (d) element mapping of magnetic carbon N-PMC.

carbons, the magnetic nanoparticles are beneficial to rapidly separate the materials from the solution. The energy dispersive X-ray spectroscopy (EDS) analysis was conducted with FE-TEM. From Fig. 3c, we can see that C, N, O and Fe peaks were obtained and their respective atomic percentages were 87.1%, 8.3%, 3.5% and 1.1%. The stoichiometric proportions of Fe_2O_3 and Fe_3C were roughly maintained. The element mapping (Fig. 3d) further shows that the C, N, O and Fe elements existed in the materials.

The porosity of the carbon N-PMC was calculated by the N_2 isotherms at 77 K. In Fig. 4a, the N-PMC shows a continuous increased N_2 adsorption with a combined feature of mixed type IV and type I isotherms. The initial sharp increase of uptake at low pressure ($p/p_0 < 0.1$) indicated a significant microporous character. The hysteresis loops under high pressure ($p/p_0 > 0.9$) demonstrated the existence of interarticular voids and macropores. The hysteresis loops under high pressure ($p/p_0 > 0.9$) demonstrated the existence of interarticular voids and macropores. The H4 hysteresis loops under the medium pressure indicate the presence of mesopores. Moreover, the curves (Fig. 4b) of pore size distribution (PSD) based on the non-local density

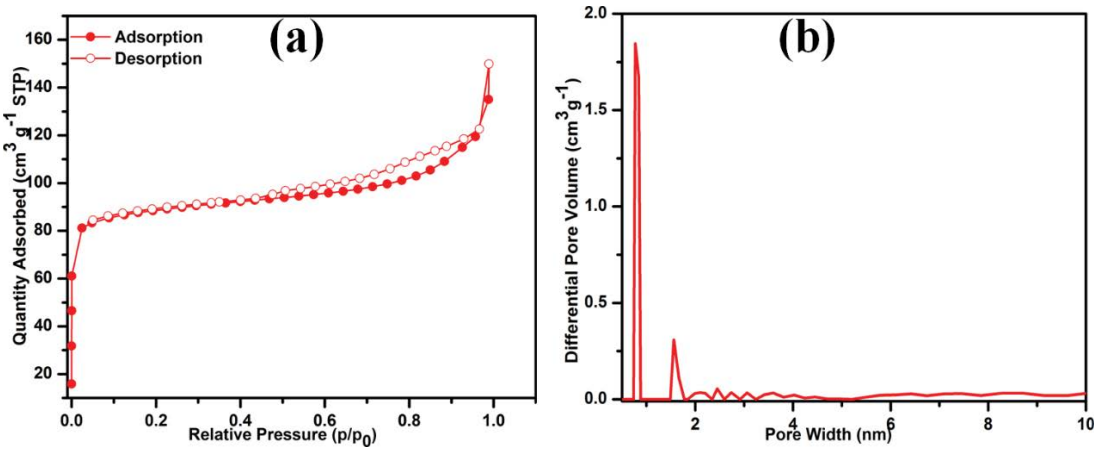

Fig. 4. (a) N_2 adsorption–desorption isotherms of N-PMC at 77 K and (b) Pore size distributions of N-PMC.

functional theory (NLDFT) also indicate that the ~1.0 nm was the main pores in the carbon. Summarized in Table S1, the BET surface area is 290.1 m^2 g^{-1} and total pore volume is 0.209 cm^3 g^{-1}.

3.2. Adsorption kinetics of MB on N-PMC

Adsorption kinetics is one of the most important characteristics that represent the adsorption efficiency of the adsorbent. [32] The time-dependent adsorption of MB on N-PMC was studied at initial concentration with 10 ppm. As shown in Fig. 5b, extremely fast kinetics is observed, which shows that it can attain 99.99% of the MB adsorption capacity at equilibrium within 1 min and is able to reduce the concentration of MB from 10 ppm to almost 0 ppm (Fig. 5a). Considering the great reliability to represent the kinetics for the adsorption of MB from aqueous solutions onto adsorbents [33], the experimental data are fitted with pseudo-second-order kinetic model:

$$\frac{t}{q_t} = \frac{1}{k_2 q_e^2} + \frac{t}{q_e} \tag{1}$$

where q_t and q_e are the adsorption capacity (mg g^{-1}) at a certain time t (min) and equilibrium, respectively. And k_2 is the rate constant for the pseudo-second-order adsorption (g mg^{-1} min^{-1}). As shown in the inset of Fig. 4b and Table S2, a very high correlation coefficient (R^2 > 0.999) is obtained for the pseudo-second-order kinetic model. This indicated that the adsorption rate of MB on N-PMC relays on the availability of adsorption sites. The value of the adsorption rate constant k_2 was determined to be 1.34 mg g^{-1} min^{-1}. This value is more than one order of magnitude higher than other adsorbent materials for MB adsorption under similar conditions [34–37]. Such extraordinarily rapid adsorption can be ascribed to its good porosity adequately to facilitate the diffusion of MB and its high surface area densely with a basic sites' nitrogen doped.

3.3. Adsorption isotherms of MB on N-PMC

As shown in Fig. 6a, with the initial concentration of MB increased, the adsorption capacity of MB gradually increased until it was equilibrium. At lower concentrations, more adsorption sites are available. With increasing MB concentration, the MB molecules occupied the available sites on the

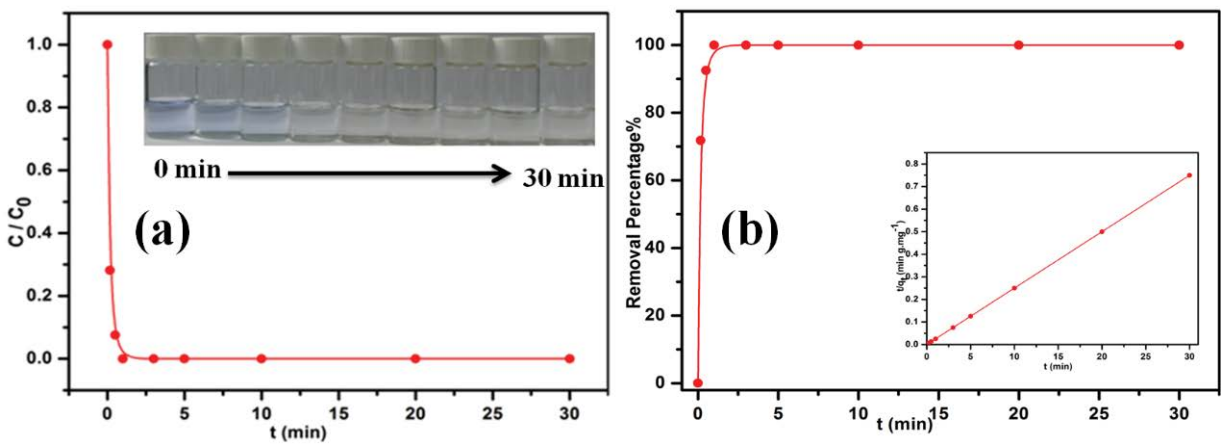

Fig. 5. (a) Adsorption rate of MB on N-PMC. The inset shows the corresponding photographs and (b) adsorption curve of MB vs. contact time on N-PMC. The inset shows the pseudo-second-order kinetics plot (C_0 = 10 mg/L, m = 2.5 mg, V = 5 mL, pH = 6.5, T = 25°C).

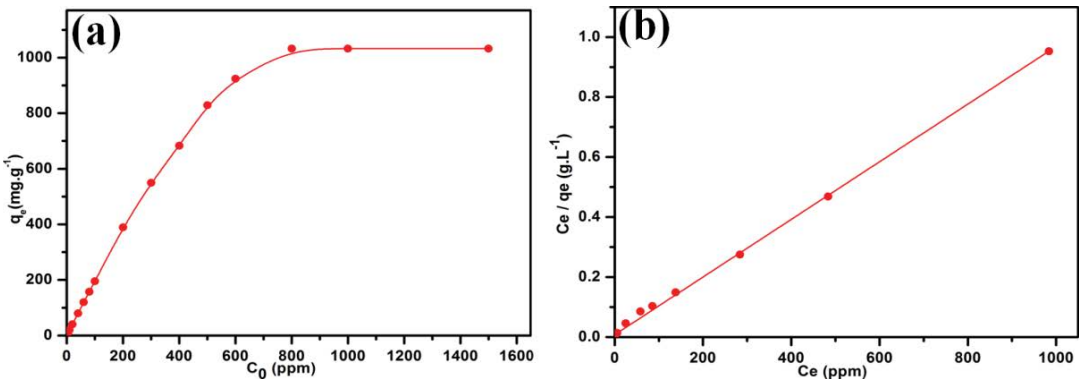

Fig. 6. (a) Adsorption isotherm of MEB on N-PMC and (b) Linear regression by fitting the equilibrium adsorption data with Langmuir adsorption model (m = 2.5 mg, V = 5 mL, t = 24 h, pH = 6.5, T = 25°C)

surface of N-PMC after reaching the maximum adsorption capacity. Therefore, the adsorption capacity of MB was at equilibrium when the MB concentrations continue to increase. The equilibrium adsorption isotherm data were fitted with Langmuir model:

$$\frac{C_e}{q_e} = \frac{C_e}{q_{\max}} + \frac{1}{q_{\max} b} \tag{2}$$

where C_e are the equilibrium concentration (mg L^{-1}) of dyes, q_e is the equilibrium adsorption capacity (mg g^{-1}) of dyes, $q_{\max}$ is the maximum adsorption capacity (mg g^{-1}) and b is the Langmuir constant. The plot of C_e/q_e against C_e gave a good linear plot initial concentration of at all the test, yielding a high correlation coefficient (R^2 = 0.998; Fig. 6b and Table S3). This reflected that the MB adsorption on N-PMC was monolayer adsorption. Remarkably, the maximum MB adsorption capacity of N-PMC was calculated to be 1,053.5 mg g^{-1}.

3.4. Comparison of adsorption capacities between different adsorbents

A comparison between N-PMC and some other previously reported adsorbents [38–41] for removing MB from aqueous solution was conducted and the results are summarized in Table 1. The maximum MB uptake capacity of N-PMC is significantly higher than that of many reported benchmark porous materials. It is worth mentioning that the adsorption capacity of N-PMC on MB is higher by three times than the analogous non-nitrogen-doped framework (PMC, 350.0 mg g^{-1}) and non-porous framework (MRF-Fe, 258 mg g^{-1}). Moreover, N-PMC is highly selective towards the acid dye MB than the basic dye MO (Fig. S4). The difference in adsorption capacity should mainly contribute to the texture parameters such as specific surface area and the properties of adsorbents. Benefitting from the highly porous structure, high specific surface area, good porosity, basic sites surface, the N-PMC shows efficient adsorption efficiency for MB. Apart from that, compared with some reported MB adsorbents, the N-PMC can be rapidly separated from the solution by an external magnet.

3.5. DFT calculation on N-PMC interaction with MB

In order to further understand its high MB adsorption capacity on N-PMC, the property and electrostatic potential (ESP) of the MB and N-PMC was conducted by the DFT calculation. The ESP of N-PMC and MB is both shown in

Table 1
Comparison of the MB adsorption capacity among various adsorbents

Adsorbents	S_{BET} (m^2 g^{-1})	$q_{\max}$ (mg g^{-1})	References
Hyper-cross-linked THPS	1,426.0	330.1	[4]
NPCNS-10	1,100.0	962.1	[19]
Bamboo-based activated carbon	1,896.0	454.2	[32]
Porous graphene oxide (PGO)	450.0	1,100.0	[34]
GO-hydrogel nanocomposites	33.0	714.3	[35]
$Co_{0.3}Ni_{0.7}Fe_2O_4$@SiO_2 membrane	32.4	107.5	[36]
Polymer organic framework BP	1,625.0	316.0	[37]
Porous carbon nanosheets (PCNSs)	2,315.0	769.2	[38]
Holey graphene nanosheets	1,053.5	269.0	[39]
N-PMC	290.1	1,053.5	This work
PMC	240.9	350.0	This work
MRF-Fe	41.1	258.0	This work

Fig. S5. As seen, the ESP MB surfaces is red color with a $V_{s,min}$ value of –135.34 kcal mol^{-1}. The carbon N-PMC is blue color with a $V_{s,max}$ value of 40.57 kcal mol^{-1}, indicating that it was more attractive with MB molecule via electrostatic interaction. In addition, the interaction energy of the N-PMC-MB complexes was also calculated. We proposed a possible adsorption model (Fig. 7). The value of the binding energy of the complexes is 96.02 kJ mol^{-1}, suggesting the strong interaction forces between molecule MB and N-PMC. Hence, the nitrogen-doped in the N-PMC skeleton may be the main contribution to the high adsorption.

3.5.1. Reuse of adsorbents

Reusing adsorbents is very important from the viewpoint of green chemistry and practical applications. The traditional reuse method involves the recovery of adsorbents by desorption using large amounts of eluent or rising with dilute HCl. Although this is an efficient process, it can lead to secondary pollution. In our work, the adsorbed dyes can be easily removed from the collected porous N-PMC by simply heating in an air atmosphere of 400°C. Then, the dried material N-PMC can be subjected to the next adsorption experiment. As shown in Fig. 8, the removal percentage of the N-PMC carbon does not significantly change during the adsorption–desorption recycle. This shows that recycling of the porous magnetic material N-PMC is a simple operation and can be recycled multiple times.

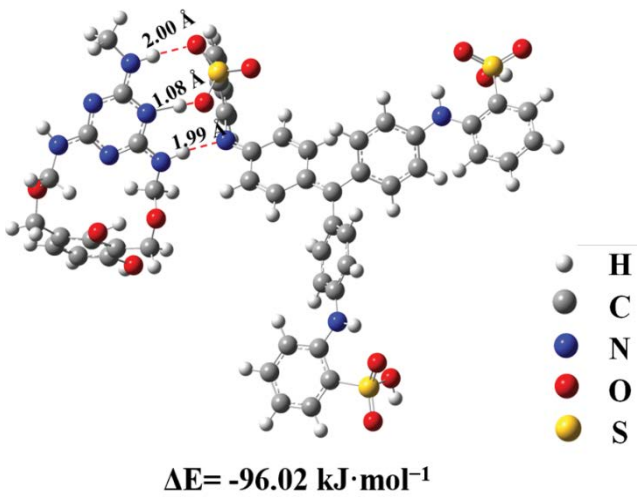

Fig. 7. Optimized geometries and interaction of N-PMC and MB.

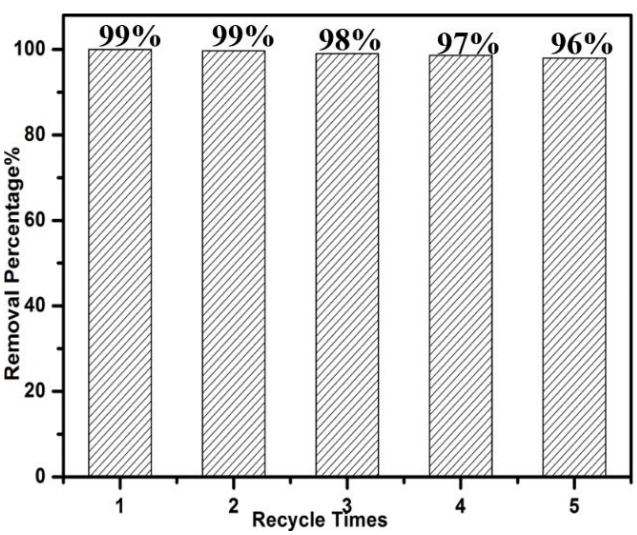

Fig. 8. Reusability of polymer N-PMC (C_0 = 10 mg/L, m = 25 mg, V = 50 mL, t = 12h, pH = 6.5, T = 25°C).

4. Conclusions

In conclusion, we reported a facile strategy for one-pot synthesis of magnetic nitrogen-doped porous carbon (N-PMC) and demonstrated its superior adsorption properties for MB removal from aqueous solution. The N-PMC showed a hierarchically porous structure, high specific surface area and the rich basic sites surface. Under optimized conditions, MB adsorption reached equilibrium within about 1 min, and the maximum adsorption capacity could be up to 1,053.5 mg g^{-1} at room temperature, which is significantly higher than those of various previously reported MB adsorbents. In addition, the as-prepared N-PMC was capable of the rapid removal and separation of MB. Furthermore, the porous magnetic carbon can be reused many times for environmental remediation through regeneration upon burning or heating in air. All these features conclude that the magnetic nitrogen-doped porous carbon N-PMC can be used as a promising adsorbent for the removal of dyes.

Conflict of interest

The authors declare no competing financial interest.

Acknowledgements

Financial support for this work was provided by the National Natural Science Foundation of China (No. 21476070, 21776069), Doctoral Scientific Research Foundation of East China University of Technology (No. DHBK2017159), China Postdoctoral Science Foundation (No. 2018M640351), the Scientific and Technical Project of the Educational Department in Jiangxi Province (GJJ180403) and the Educational Department in Jiangxi Province and the Opening Project of Jiangxi Province Key Laboratory of Polymer Micro/Nano Manufacturing and Devices (No. 2018-398-10).

References

[1] Y. Shao, X. Wang, Y. Kang, Y. Shu, L Li, Application of Mn/MCM-41 as an adsorbent to remove methyl blue from aqueous solution, J. Colloid Interface Sci., 429 (2014) 25–33.
[2] H. Karaer, I. Uzun, Adsorption of basic dyestuffs from aqueous solution by modified chitosan, Desal. Wat. Treat., 51 (2013) 2294–2305.
[3] S. Chen, S. Tang, Y. Sun, G. Wang, H. Chen, X. Yu, Y. Su, G. Chen, Preparation of a highly porous carbon material based on quinoa husk and its application for removal of dyes by adsorption, Materials, 11 (2018) 1407–1410.
[4] C. Zhang, P.C. Zhu, L. Tan, J.M. Liu, B.E. Tan, X.L. Yang, H.B. Xu, Triptycene-based hyper-cross-linked polymer sponge

for gas storage and water treatment, Macromolecules, 48 (2015) 8509–8514.
[5] N. Sarkar, G. Sahoo, R. Das, Three-dimensional rice straw-structured magnetic nanoclay-decorated tripolymeric nanohydrogels as super adsorbent of dye pollutants, ACS Appl. Nano Mater., 1 (2018) 1188–1203.
[6] C. Li, Y. He, L. Zhou, C.J. Peng, H.L. Liu, Fast adsorption of methylene blue, basic fuchsin, and malachite green by a novel sulfonic-grafted triptycene-based porous organic polymer, RSC Adv., 73 (2018) 41986–41993.
[7] M.M. Khin, A.S. Nair, V.J. Babu, A review on nanomaterials for environmental remediation, Energy Environ. Sci., 5 (2012) 8075–8109.
[8] A. Alsbaiee, B.J. Smith, L. Xiao, Rapid removal of organic micropollutants from water by a porous β-cyclodextrin polymer, Nature, 529 (2016) 190–193.
[9] I. Ali, New generation adsorbents for water treatment, Chem. Rev., 112 (2012) 5073–5091.
[10] R.X. Yang, T.T. Wangand, W.Q. Deng, Extraordinary capability for water treatment achieved by a perfluorous conjugated microporous polymer, Sci. Rep., 5 (2015) 12–15.
[11] M. Zhao, Z. Tang, P. Liu, Removal of methylene blue from aqueous solution with silica nano-sheets derived from vermiculite, J. Hazard. Mater., 158 (2008) 43–51.
[12] L. Huang, M. He, B. Chen, Facile green synthesis of magnetic porous organic polymers for rapid removal and separation of methylene blue, ACS Sustain. Chem. Eng., 5 (2017) 4050–4055.
[13] A. Asfaram, M. Ghaedi, S. Hajati, A. Goudarzi, E.A. Dil, Screening and optimization of highly effective ultrasound-assisted simultaneous adsorption of cationic dyes onto Mn-doped Fe_3O_4-nanoparticle-loaded activated carbon, Ultrason. Sonochem., 34 (2017) 1–12.
[14] H.N. Abdelhamid, X. Zou, Template-free and room temperature synthesis of hierarchical porous zeolitic imidazolate framework nanoparticles and their dye and CO_2 sorption, Green Chem., 20 (2018) 1074–1084.
[15] Y. Wang, J. Xie, Y. Wu, H. Ge, X. Hu, Preparation of a functionalized magnetic metal-organic framework sorbent for the extraction of lead prior to electrothermal atomic absorption spectrometer analysis, J. Mater. Chem. A, 31 (2013) 8782–8789.
[16] S.L. Candelaria, B.B. Garcia, D. Liu, Nitrogen modification of highly porous carbon for improved supercapacitor performance, J. Mater. Chem., 19 (2012) 9884–9889.
[17] L. Yang, S. Jiang, Y. Zhao, Boron-doped carbon nanotubes as metal-free electrocatalysts for the oxygen reduction reaction, Angew. Chem. Int. Ed., 31 (2011) 7270–7273.
[18] Z. Qian, X. Shan, L. Chai, Si-doped carbon quantum dots: a facile and general preparation strategy, bioimaging application, and multifunctional sensor, ACS Appl. Mater. Inter., 9 (2014) 6797–6805.
[19] Y. He, H. Li, L. Zhou, C.J. Peng, H.L. Liu, Removal of methyl orange from aqueous solutions by a novel hyper-cross-linked aromatic triazine porous polymer, Acta Phys.-Chim. Sinica, 35 (2018) 299–306.
[20] D.S. Yang, D. Bhattacharjya, S. Inamdar, Phosphorus-doped ordered mesoporous carbons with different lengths as efficient metal-free electrocatalysts for oxygen reduction reaction in alkaline media, J. Am. Chem. Soc., 39 (2012) 16127–16130.
[21] W. Shen, W. Fan, Nitrogen-containing porous carbons: synthesis and application, J. Mater. Chem. A, 4 (2013) 999–1013.
[22] G. Yang, L. Tang, G. Zeng, Simultaneous removal of lead and phenol contamination from water by nitrogen-functionalized magnetic ordered mesoporous carbon, Chem. Eng. J., 259 (2015) 854–864.
[23] Q. Li, J. Zhang, Q. Lu, Hydrothermal synthesis and characterization of ordered mesoporous magnesium silicate-silica for dyes adsorption, Mater. Lett., 170 (2016) 167–170.
[24] M.J. Frisch, G.W. Trucks, H.B. Schlegel, G.E. Scuseria, M.A. Robb, J.R. Cheeseman, G. Scalmani, V. Barone, B. Mennucci, G.A. Petersson, Gaussian 09; Gaussian Inc., Wallingford, CT, 2009.
[25] T. Xu, Y. He, Y. Qin, C.J. Peng, H.L. Liu, Facile preparation of porous organic copolymer based on triptycene and crown ether for efficient organic dye adsorption, RSC Adv., 8 (2018) 4963–4968.
[26] Y. Li, Q. Meng, S.M. Zhu, Z.H. Sun, H. Yang, Z.X. Chen, C.L. Zhu, Z.P. Guo, D. Zhang,. A Fe/Fe_3O_4/N-carbon composite with hierarchical porous structure and in situ formed N-doped graphene-like layers for high-performance lithium ion batteries, Dalton Trans., 10 (2015) 4594–4600.
[27] B.H. Kim, N. Lee, H. Kim, K. An, Y.I. Park, Y. Choi, K. Shin, Y. Lee, S.G. Kwon, H.B. Na, J.G. Park, T.Y. Ahn, Y.W. Kim, W.K. Moon, S.H. Choi, T. Hyeon, Large-scale synthesis of uniform and extremely small-sized iron oxide nanoparticles for high-resolution T 1 magnetic resonance imaging contrast agents, J. Am. Chem. Soc., 133 (2011) 12624–12631.
[28] D.H. Liu, Y. Guo, L.H. Zhang, W.C. Li, T. Sun, A.H. Lu, Switchable transport strategy to deposit active Fe/Fe_3C cores into hollow microporous carbons for efficient chromium removal, Small, 22 (2013) 3852–3857.
[29] Y. Ma, G. Ji, J.Y. Lee, Synthesis of mixed-conducting carbon coated porous γ-Fe_2O_3 microparticles and their properties for reversible lithium ion storage, J. Mater. Chem., 21 (2011) 13009–13014.
[30] M. Descostes, F. Mercier, N. Thromat, Use of XPS in the determination of chemical environment and oxidation state of iron and sulfur samples: constitution of a data basis in binding energies for Fe and S reference compounds and applications to the evidence of surface species of an oxidized pyrite in a carbonate medium, Appl. Surf. Sci., 165 (2000) 288–302.
[31] X.M. Sun, Y.D. Li, Colloidal carbon spheres and their core/shell structures with noble metal nanoparticles, Angew. Chem. Int. Ed., 43 (2004) 597–601.
[32] S. Wang, Y.Y. Zhai, Q. Gao, Highly efficient removal of acid red 18 from aqueous solution by magnetically retrievable chitosan/carbon nanotube: batch study, isotherms, kinetics, and thermodynamics, J. Chem. Eng. Data, 59 (2013) 39–51.
[33] Y.S. Ho Review of second-order models for adsorption systems, J. Hazard. Mater., 136 (2006) 681–689.
[34] B.H. Hameed, A.T.M. Din, A.L. Ahmad, Adsorption of methylene blue onto bamboo-based activated carbon: kinetics and equilibrium studies, J. Hazard. Mater., 141 (2007) 819–825.
[35] S. Altenor, B. Carene, E. Emmanuel, J. Lambert, J.J. Ehrhardt, S. Gaspard, Adsorption studies of methylene blue and phenol onto vetiver roots activated carbon prepared by chemical activation, J. Hazard. Mater., 165 (2009) 1029–1039.
[36] D.E. Kong, X.Y. Zheng, Y. Tao, W. Lv, Y. Gao, L.J. Zhi, Q.H. Yang, Porous graphene oxide-based carbon artefact with high capacity for methylene blue adsorption, Adsorption, 22 (2016) 1043–1050.
[37] A. Pourjavadi, M. Nazari, B. Kabiri, S.H. Hosseini, C. Bennett, Preparation of porous graphene oxide/hydrogel nanocomposites and their ability for efficient adsorption of methylene blue, RSC Adv., 13 (2016) 10430–10437.
[38] Z.G. Zhu, G.H. Li, G.F. Zeng, X.Q. Chen, D. Hu, Y.F. Zhang, Y.H. Sun. Fast capture of methyl-dyes over hierarchical amino-$Co_{0.3}Ni_{0.7}Fe_2O_4$@SiO_2 nanofibrous membranes, J. Mater. Chem. A, 44 (2015) 22000–22004.
[39] P. Kuhn, K. Krüge, A. Thomas, M. Antonietti, "Everything is surface": tunable polymer organic frameworks with ultrahigh dye sorption capacity, Chem. Commun., 44 (2008) 5815–5817.
[40] J. Gong, J. Liu, X.C. Chen, Z.W. Jiang, X. Wen, E. Mijowska, T. Tang, Converting real-world mixed waste plastics into porous carbon nanosheets with excellent performance in the adsorption of an organic dye from wastewater, J. Mater. Chem. A, 3 (2015) 341–351.
[41] Z.C. Xing, J.Q. Tian, Q. Liu, A.M. Asiri, P. Jiang, X.P. Sun, Holey graphene nanosheets: large-scale rapid preparation and their application toward highly-effective water cleaning, Nanoscale, 20 (2014) 11659–11663.

Supplementary information

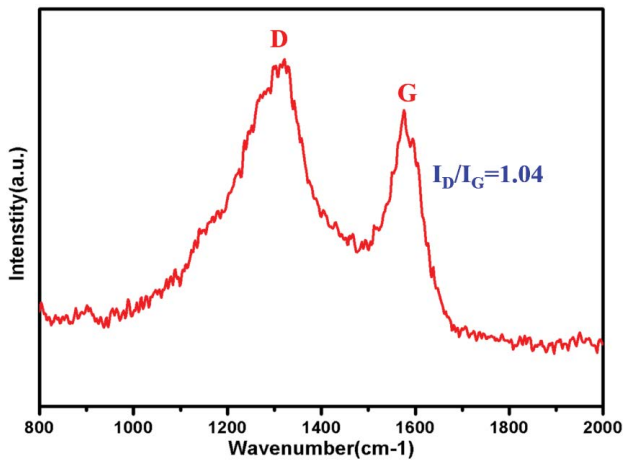

Fig. S1. Raman spectrum of N-PMC.

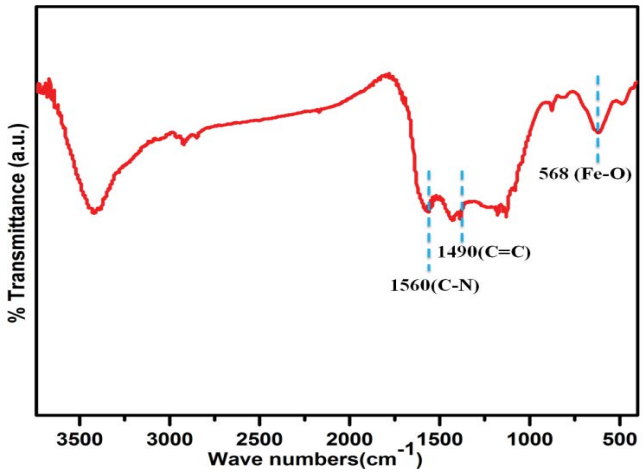

Fig. S2. FTIR spectrum of magnetic polymer N-PMC.

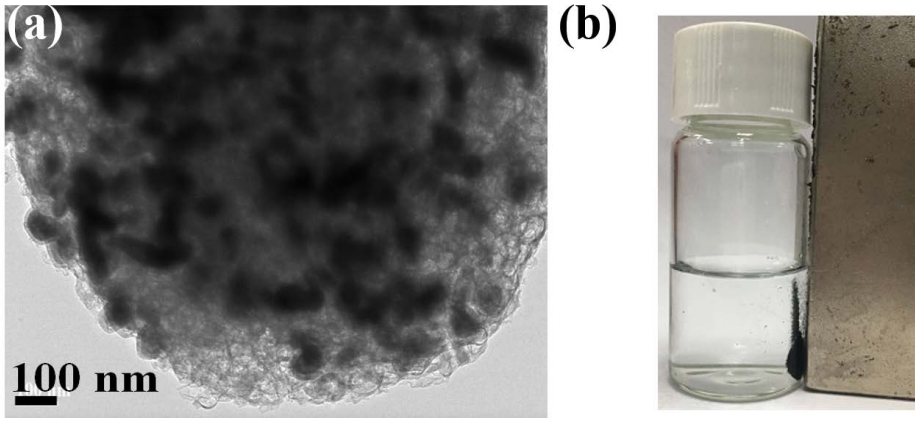

Fig. S3. (a) HR-TEM image of N-PMC; (b) photograph of N-PMC isolated by an external magnet within several seconds.

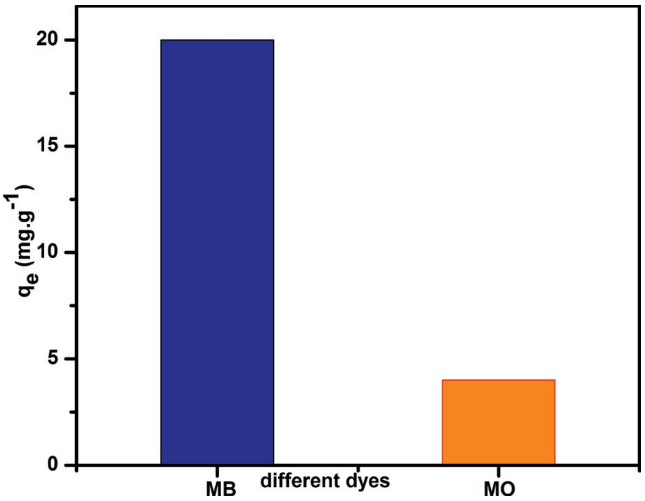

Fig. S4. Different dyes adsorption on the polymer N-PMC (C_0 = 10 ppm, m = 2.5 mg, V = 5 mL).

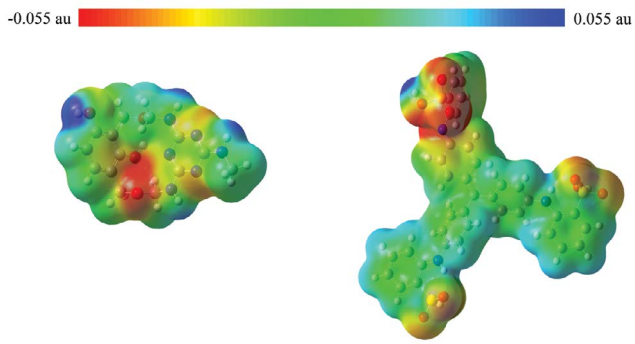

Fig. S5. Computed electrostatic potential at isodensity contour surface of N-PMC and MB.

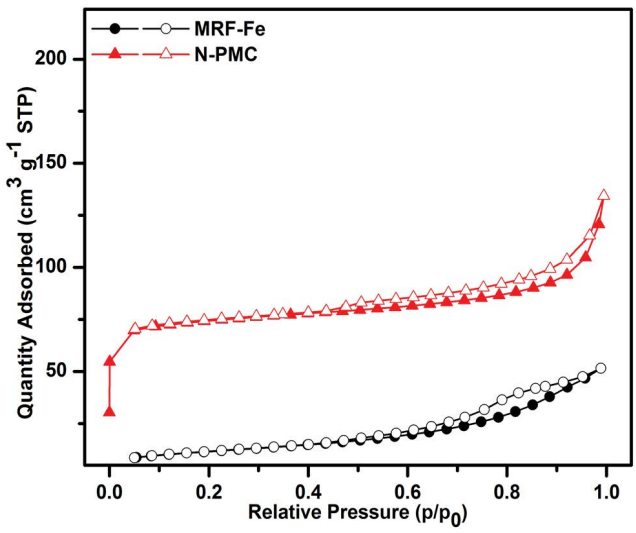

Fig. S6. N_2 adsorption–desorption isotherms of N-PMC and MRF-Fe at 77 K.

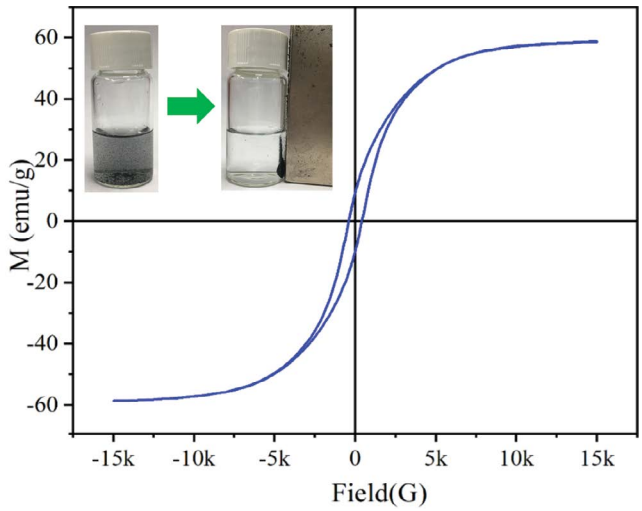

Fig. S8. Magnetic hysteresis loop of N-PMC with photographs reflecting the magnetic separability and water dispersity of N-PMC (the top inset).

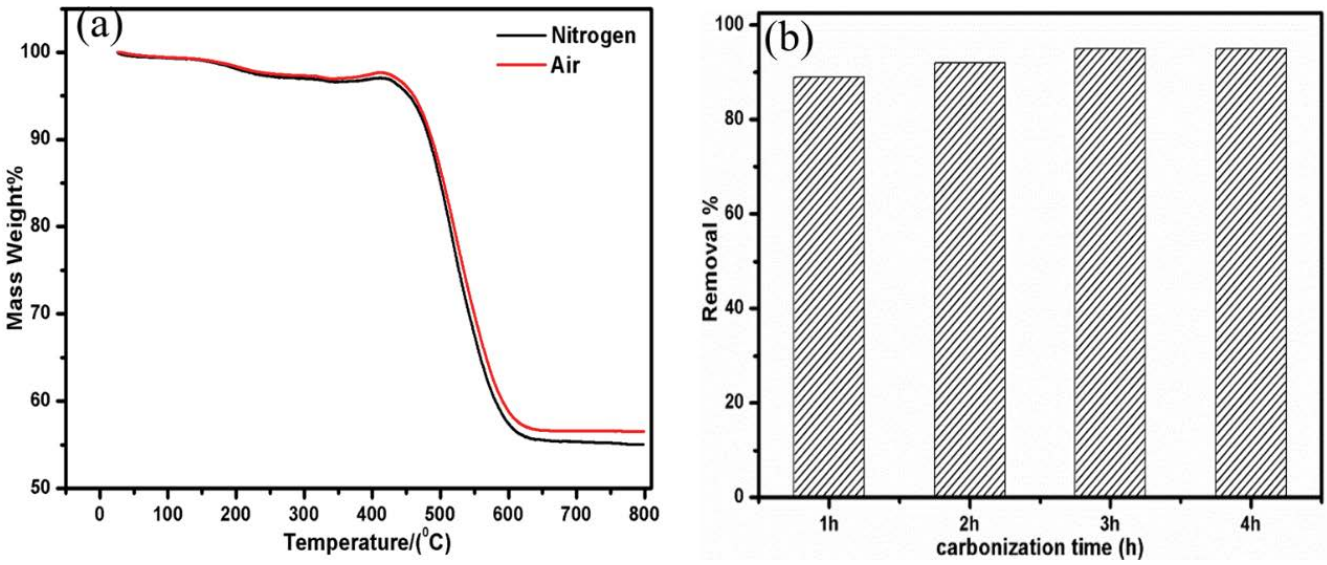

Fig. S7. (a) TG of N-PMC and (b) effect of carbonization time for the N-PMC reusability.

Table S1
Porosity properties of magnetic polymer N-PMC

Polymer	SA_{BET} [a] ($m^2\ g^{-1}$)	V_t [b] ($cm^3\ g^{-1}$)	V_m [c] ($cm^3\ g^{-1}$)	% V_m/V_t
N-PMC	290.1	0.2088	0.1125	53.8

[a]Specific surface area calculated from the nitrogen adsorption isotherm using the BET method.
[b]Total pore volume at $p/p_0 = 0.987$.
[c]Micropore volume derived from the *t*-plot method.

Table S2
Pseudo-first-order and pseudo-second-order kinetic model parameters of N-PMC

	Pseudo-first-order			Pseudo-second-order		
$q_{e,\exp}$ (mg g^{-1})	k_1 (min^{-1})	$q_{e,\text{cal}}$ (mg g^{-1})	R^2	k_2 (g mg^{-1} min^{-1})	$q_{e,\text{cal}}$ (mg g^{-1})	R^2
19.9	0.00456	6.717	0.77178	1.34	20.01	0.99999

Table S3
Isotherm parameters of Langmuir and Freundlich models

Freundlich parameters			Langmuir parameters		
K	n	R^2	$q_{\max}$ (mg g^{-1})	b (L mg^{-1})	R^2
6.15	1.9047	0.95478	1,053.5	0.05694	0.998